Removal of Methyl Orange from Aqueous Solutions by Magnetic Maghemite/Chitosan Nanocomposite Films: Adsorption Kinetics and Equilibrium

Ru Jiang,[1] Yong-Qian Fu,[1] Hua-Yue Zhu,[1,2] Jun Yao,[1] Ling Xiao[2]

[1]College of Life Science, Taizhou University, Linhai 317000, People's Republic of China
[2]Key Laboratory for Biomass-Resource Chemistry and Environmental Biotechnology of Hubei Province, College of Resource and Environmental Science, Wuhan University, Wuhan 430072, People's Republic of China

ABSTRACT: Magnetic maghemite (γ-Fe$_2$O$_3$)/chitosan nanocomposite films were prepared by solution casting method and characterized by Fourier transform infrared spectra, thermogravimetric analysis, differential scanning calorimetry and X-ray diffraction. Batch adsorption experiments were carried out utilizing the composite films to adsorb a typical azo dye, i.e., methyl orange (MO) from aqueous solutions. The effects of adsorbent dosage, solution pH, coexisting anions, and temperature were studied. Adsorption kinetic was verified by pseudo-first-order and pseudo-second-order kinetic models. Results indicated that the rate of dye adsorption followed pseudo-second-order kinetic model for the initial dye concentration range studied. MO adsorption onto magnetic γ-Fe$_2$O$_3$/chitosan composite films was better described by Langmuir isotherm. Thermodynamic studies showed that MO adsorption was exothermic and spontaneous in nature. Because magnetic maghemite/chitosan nanocomposite films could be recovered conveniently and possessed of excellent adsorptive property, it can be developed as an economical and alternative adsorbent to decolorize or treat dye wastewater. © 2012 Wiley Periodicals, Inc. J Appl Polym Sci 000: 000–000, 2012

Key words: chitosan; adsorption; magnetic separation; methyl orange; maghemite

INTRODUCTION

Wastewater effluents from different industries, such as textiles, rubber, paper, and plastics, contain several kinds of synthetic dyestuffs.[1] The release of these colored waters to the environment is a considerable source of nonaesthetic pollution and eutrophication. Because of the complex aromatic structure and the stability of these dyes, conventional biological treatment methods are ineffective for decolorization.[2] Other commonly used techniques for dye decolorization include flocculation, membrane filtration, and reverse osmosis.[3–5] However, these methods are merely transferring the contaminants from liquid phase to other media and causing secondary pollution. Photocatalytic oxidation process is a destructive technology leading to the total mineralization of most organic dyes.[6] The drawbacks of photocatalytic oxidation technology are mainly the ineffective utilization of economic and ecological sunlight and high electron-hole pair recombination rate. Adsorption on activated carbon appears to be the best prospect of dye removal. Despite its high efficiency, this adsorbent is expensive and difficult to regenerate.

Adsorption on locally available, low cost waste materials for dye removal is quite popular due to simplicity and high efficiency. Chitosan, a biopolymer of glucosamine, exhibits a higher adsorption capacity of dyes than activated carbon.[7] Additionally, chitosan is economically attractive because it is the second abundant biopolymer in nature, obtained from the shells of shrimp, crabs, and lobsters, which are waster products of seafood processing industries. However, raw chitosan presents some major difficulties in adsorption process, i.e. (i) unsatisfactory mechanical properties and poor heat resistance, (ii) dissolution in acidic media, (iii) high swelling ratios, which limits its use in columns,[8] and (iv) difficulty in recovery. To overcome the first three limitations, cross-linking can improve the stability of chitosan. While for the last limitation, chitosan is frequently found as flakes or films for dye removal to simplify the recovery procedure due to its excellent film forming property.

Recently, the application of magnetic adsorption technology to solve environmental problems has

received considerable attention. After magnetic adsorbents are used to adsorb contaminants from aqueous solutions, they can be separated conveniently from the medium by a simple magnetic process.[9] Many researchers have focused on the removal of organic pollutant by magnetic materials adsorption based on the magnetite (Fe_3O_4) or hematite (α-Fe_2O_3).[10–12] Because of its excellent chemical stability and magnetic properties,[13] some composite adsorbents based on maghemite (γ-Fe_2O_3), such as chitosan/γ-Fe_2O_3/fly-ash composite, chitosan/γ-Fe_2O_3/kaolin composite, γ-Fe_2O_3/Al_2O_3, and γ-Fe_2O_3/polymer composites are also reported.[14–17]

However, there have few reports on magnetic cross-linked chitosan based on maghemite (γ-Fe_2O_3), i.e. γ-Fe_2O_3/chitosan composite as adsorbent for dye removal. In our laboratory, the preparation and characterization of γ-Fe_2O_3/crosslinked chitosan composite particles by water-in-oil microemulsion process were reported.[18] It has been approved that magnetic γ-Fe_2O_3/crosslinked chitosan composite particles exhibited faster adsorption rate toward methyl orange (MO) compared with cross-linked chitosan and could be separated and recovered conveniently by applying an adscititious magnetic field. Nevertheless, many organic solvents were involved during the microemulsion process, leading to complicated preparation procedure, high operation cost, and secondary pollution.
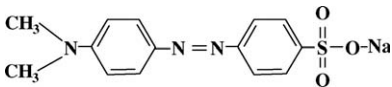
In this study, solution casting method was applied to prepare magnetic γ-Fe_2O_3/chitosan composite films based on the highly viscous nature and excellent film forming property of chitosan. MO was also selected as a model pollutant to examine the adsorption capacity. The effect of key operational factors, i.e., adsorbent amount, solution pH, coexisting anions, and temperature on dye removal has been researched systematically. The adsorption kinetics, isotherms, and thermodynamics were also studied.

EXPERIMENTAL

Materials

Chitosan with 91.7% degree of deacetylation (DD) and molecular weight of 2.1×10^5 was purchased from Yuhuan Ocean Biology Company (Zhejiang, China). Commercially available magnetic γ-Fe_2O_3 nanoparticles with 98% purity (20-30 nm outer diameters) were provided by Tongrenweiye Technology Co., Ltd. (Hebei, China). MO obtained from Yongjia Fine Chemical Factory (Zhejiang, China) was used as an adsorbate. Its chemical structure and other characteristics are listed in Table I. All the other reagents used are of analytical grade. Double distilled water was used throughout the study.

TABLE I
Structure and Characteristics of Methyl Orange

Methyl orange	
Structure	
Other name	Acid orange 52
C.I. number	13,025
λ_{max} (nm)	464.9
MW (g/mol)	327.33

Preparation of magnetic γ-Fe_2O_3/chitosan composite films

Magnetic γ-Fe_2O_3/chitosan composite films were prepared by solution casting method. A total of 0.5 g commercial magnetic γ-Fe_2O_3 nanoparticles were dispersed into 100 mL of 2% (w/v) chitosan-dilute acetic acid colloidal solution with continuous ultrasonically stirring for 30 min. Then the viscous mixture solution was poured and cast onto clean and dry glass plates to form uniform films, and dried at room temperature. The dried films as well as the glass plates were immersed into 0.2 mol L^{-1} NaOH solution and the films were flaked away from the glass plates. To improve the acid resistance of the composite films, 2% (v/v) of glutaraldehyde solution was added dropwise with continuous stirring for 30 min in a water bath at 60°C. Finally, the obtained films were washed by alcohol, N, N-dimethylformamide and double distilled water for two times, respectively, and dried in an oven at 60°C till constant weight.

Characterization of samples

Fourier transform infrared (FTIR) spectra were measured at room temperature on a FTIR-8400 spectrometer (Shimadzu, Japan). Thermogravimetric analysis (TGA) and differential scanning calorimetry (DSC) were performed in a Setaram Setsys 16 TG/DTA/DSC (France) under a nitrogen atmosphere from 25°C to 800°C with a heating rate of 2°C min^{-1}. X-ray diffraction (XRD) patterns were obtained in ambient air at room temperature using a Bruker D8 Advance diffractometer with Cu-Kα. The accelerating voltage, emission current, and scanning speed were 40 kV, 40 mA, and 6 degree min^{-1}, respectively.

Batch adsorption experiment

A stock solution of dye of concentration 1 g L^{-1} was prepared by dissolving 0.5 g of solid dye in 500 mL of double distilled water. The desired concentrations ranging from 10 to 60 mg L^{-1} were obtained by dilution. The adsorption of MO was performed by batch technique in conical flasks at (37±1)°C. A

certain amount of magnetic γ-Fe$_2$O$_3$/chitosan composite films were suspended in 50 mL of MO aqueous solutions of predetermined concentration. The mixture was agitated at 100 rpm in a thermostated rotary shaker (KYC-1102C, Ningbo Jiangnan Instrument Factory, China). At given time intervals, the suspension containing adsorbents was extracted and adsorbents were collected using an adscititious magnet. Then the residual MO concentration in supernate after magnetic separation was monitored by colorimetric method.

Mensuration of dye concentration and error analysis

Dye concentration was determined colorimetrically by measuring at maximum adsorbance of 464.9 nm using a Cary 50 UV–vis spectrophotometer (Varian, USA). A calibration curve was plotted between absorbance and concentration of the dye solution to obtain an absorbance–concentration profile. The instant dye concentration was determined through the calibration curve.

The amount of MO adsorbed on magnetic γ-Fe$_2$O$_3$/chitosan composite films at a predetermined time t, q_t (mg g^{-1}), was determined using the mass balance equation:

$$q_t = \frac{(C_0 - C_t)V}{m}. \tag{1}$$

The decolorization rate (η) of MO can be calculated by the following equation:

$$\eta = \frac{(C_0 - C_t)}{C_0} \times 100(\%) \tag{2}$$

where C_0 is the initial concentration of MO (mg L^{-1}), C_t is the instant concentration of MO at a predetermined time t (mg L^{-1}), V is the volume of solution (L), and m is the mass of magnetic γ-Fe$_2$O$_3$/chitosan composite films (g).

Because of the inherent bias resulting from linearization of the isotherm model, the nonlinear regression chi-square (χ^2) test was performed as a criterion for the quality of fitting of all the isotherm models. The χ^2 test statistic is basically the sum of the squares of the differences between the experimental data and the data obtained by calculating from models, with each squared difference divided by the corresponding data calculated using the models.[19] This can be represented mathematically as:

$$\chi^2 = \sum \frac{(q_{e,\exp} - q_{e,\mathrm{cal}})^2}{q_{e,\mathrm{cal}}} \tag{3}$$

where $q_{e,\exp}$ is the equilibrium adsorption capacity from the experiment (mg g^{-1}) and $q_{e,\mathrm{cal}}$ is the calcu-
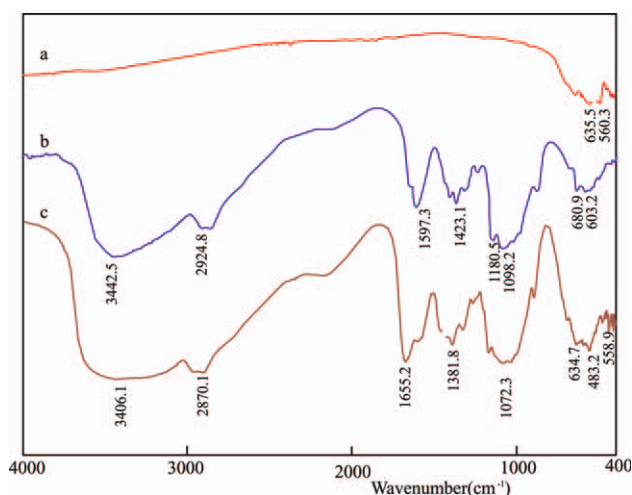
Figure 1 FTIR spectra of γ-Fe$_2$O$_3$ (a), chitosan (b), and magnetic γ-Fe$_2$O$_3$/chitosan composite films. [Color figure can be viewed in the online issue, which is available at wileyonlinelibrary.com].

lated equilibrium capacity from the isotherm model (mg g^{-1}). A small value of χ^2 indicates that data from the model is similar to the experimental value, whereas a large value of χ^2 points out the difference between them.[20,21] Therefore, it is necessary to analyze the data using the χ^2 test, combined with the values of the correlation coefficients, to confirm the best-fit isotherm and kinetic model.

RESULTS AND DISCUSSION

Characterization of the composite films

FTIR

The FTIR spectra of γ-Fe$_2$O$_3$ (a), chitosan (b), and magnetic γ-Fe$_2$O$_3$/chitosan composite films (c) were shown in Figure 1. For magnetic γ-Fe$_2$O$_3$ nanoparticles [Fig. 1(a)], peaks at 560 and 636 cm^{-1} related to Fe—O group.[11] Characteristic peaks assignment of chitosan [Fig. 1(b)] were as follows: 1597 cm^{-1} (amide II band, N—H stretch), 2925 cm^{-1} (C—H stretch), and 3442 cm^{-1} (N—H stretch overlapped with O—H stretch). It was remarkable that the absorption peak of the amide I at 1650 cm^{-1} was weak in the IR spectrum of chitosan [Fig. 1(b)], indicating that the raw chitosan possesses higher deacetylation degree. Compared with the spectra of γ-Fe$_2$O$_3$ [Fig. 1(a)] and chitosan [Fig. 1(b)], the spectrum of magnetic γ-Fe$_2$O$_3$/chitosan composite films [Fig. 1(c)] showed broader band at 3150–3700 cm^{-1}, which was attributed to hydroxyl (O—H) stretching. Secondly, the spectrum of magnetic γ-Fe$_2$O$_3$/chitosan composite films displayed a disappearance of the band at 1596 cm^{-1} and the buildup of the fresh stretching vibration characteristic peak of C=N appeared at 1655 cm^{-1}, which was related to the cross-linking
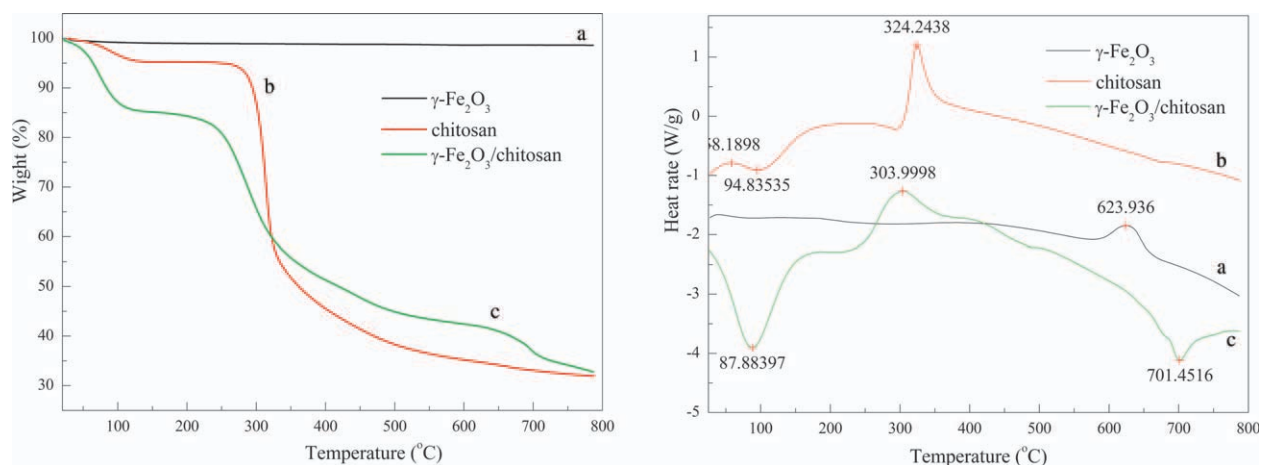
Figure 2 TG (left) and DSC (right) curves of γ-Fe₂O₃ (a), chitosan (b), and magnetic γ-Fe₂O₃/chitosan composite films (c). [Color figure can be viewed in the online issue, which is available at wileyonlinelibrary.com].

reaction by glutaraldehyde.[22] Thirdly, two sharp peaks at 559 and 635 cm^{-1} related to Fe—O group appeared, that might be attributed to the introduction of γ-Fe₂O₃. Thus, the results of FTIR analysis suggested that the γ-Fe₂O₃ nanoparticles have been successfully bonded into cross-linked chitosan films by amide linkage.

TG and DSC analysis

Figure 2 exhibited the TG (left) and DSC (right) curves for γ-Fe₂O₃ (a), chitosan (b), and magnetic γ-Fe₂O₃/chitosan composite films (c), respectively. It was obvious that TG curves of both chitosan and magnetic γ-Fe₂O₃/chitosan composite films had two main stage of weight loss in the range of 20–600°C. The first stage of chitosan was in the range of 20–140°C with weight loss ∼ 4.7%, whereas the first stage of magnetic γ-Fe₂O₃/chitosan composite films was in the range of 26–141°C with weight loss of 14.8%. Generally, the weight loss in the first stage resulted from the loss of water in the materials.[23] The second weight loss was observed between 200°C and 400°C (chitosan: from 277°C to 390°C, and magnetic γ-Fe₂O₃/chitosan composite films: from 207°C to 364°C), as seen from the exothermic peak at 324°C and 304°C in the DSC curves, respectively. The weight loss of magnetic γ-Fe₂O₃/chitosan composite films was shifted to lower temperatures than that of chitosan in the second stage. Such a shift to lower temperature was attributed to a decrease in thermal stability as a consequence of the weakening of inter- and extra-molecular hydrogen bonding in magnetic γ-Fe₂O₃/chitosan composite films.[24] Compared with TG and DSC curves of chitosan, further weight loss of magnetic γ-Fe₂O₃/chitosan composite films took place in the range of 625–740°C with weight loss of 8%, while an peak was observed at 701°C in the DSC curve. In fact, there

was an exothermic peak at 624°C in the DSC curve of γ-Fe₂O₃, which represented the phase transition from γ-Fe₂O₃ to α-Fe₂O₃.[25] The results indicated that the structure of chitosan chains has been changed due to the introduction of magnetic γ-Fe₂O₃ and the reduced ability of crystallization. However, the composite adsorbent still can meet the basic thermal qualifications as an excellent adsorbent for the removal of MO from aqueous solutions because adsorption treatment was carried out under normal temperature.

XRD

The phase and purity of γ-Fe₂O₃ (a) and magnetic γ-Fe₂O₃/chitosan composite films (b) were determined by XRD measurements, as shown in Figure 3. For XRD pattern of γ-Fe₂O₃, the diffraction peaks at
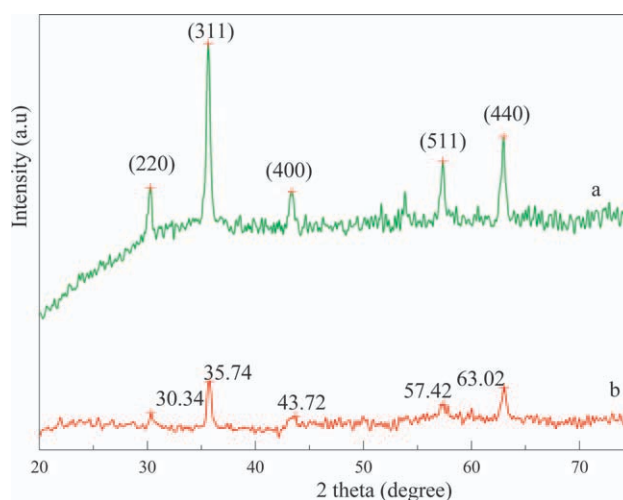
Figure 3 XRD patterns of γ-Fe₂O₃ (a) and magnetic γ-Fe₂O₃/chitosan composite films (b). [Color figure can be viewed in the online issue, which is available at wileyonlinelibrary.com].
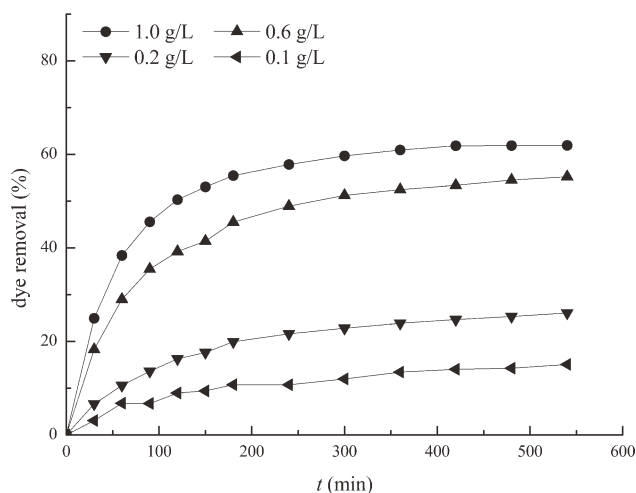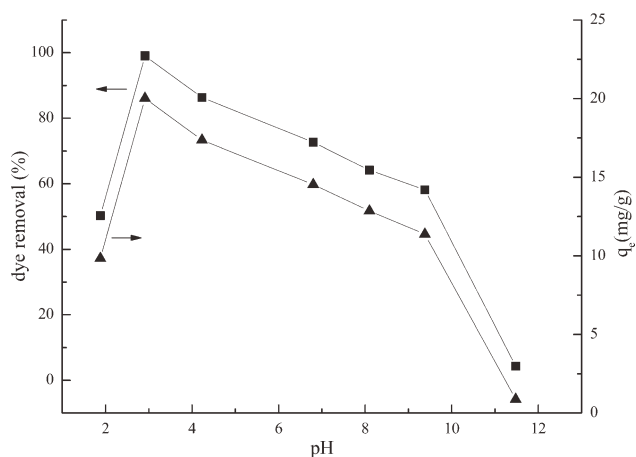
Figure 4 Effect of adsorbent dosage on color removal of MO. $C_0 = 20$ mg/L, agitation speed $= 100$ rpm, temperature $= 310$ K, pH $= 5.6$.

$30.36°$, $35.64°$, $43.36°$, $57.34°$, and $62.98°$ were corresponding to the (220), (311), (400), (511), and (440) crystal planes of pure γ-Fe$_2$O$_3$ (JCPDS No. 39-1346).[26,27] No other impurities including α-phase Fe$_2$O$_3$ were found in the samples. As for the XRD pattern of magnetic γ-Fe$_2$O$_3$/chitosan composite films, all of the peaks could be readily indexed to γ-phase of Fe$_2$O$_3$ though the intensity of all characteristic peaks became weaker than those of the γ-Fe$_2$O$_3$. Therefore, the result of XRD analysis indicated that γ-Fe$_2$O$_3$ has been introduced into chitosan films.

Effect of operational parameters on dye removal

Effect of adsorbent dosage

Adsorbent dosage is an important parameter because it determines the capacity of an adsorbent for a given initial concentration of the adsorbate.
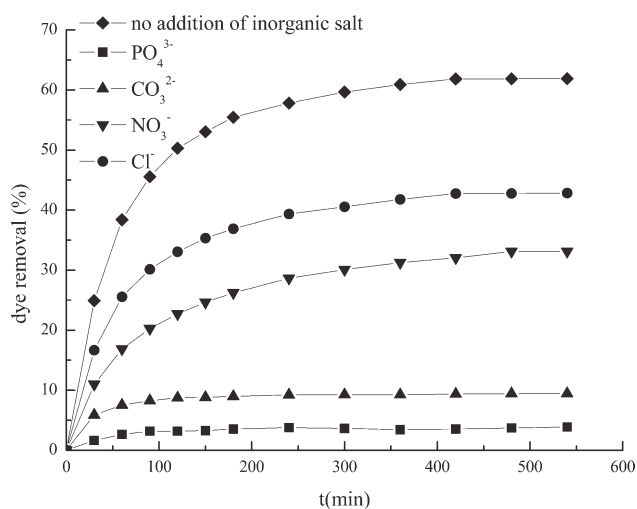
The dependence of adsorbent dosage on the adsorption of dye was studies and the results are shown in Figure 4.

The percentage of color removal increased as adsorbent dosage increased. The percentage of color removal has more than doubled (increased from 26.09% to 55.21%) after 540 min of reaction by increasing adsorbent dosage from 0.2 to 0.6 g L^{-1}. As adsorbent dosage was further increased to 1.0 g L^{-1}, the percentage of color removal only increased by 6.7%. It also showed that the amount of MO adsorbed decreased from 28.97 to 12.39 mg g^{-1} as the adsorbent dosage was increased from 0.1 to 1.0 g L^{-1}. For a certain initial solute concentration, increasing the adsorbent dosage provided more adsorption sites available for adsorbent–adsorbate interaction,[28] whereas the decrease in the amount of adsorbate adsorbed per unit mass of adsorbent (mg g^{-1}) was due to adsorption sites remaining unsaturated during the adsorption process.

Effect of medium pH

Experiments were carried out in the pH range of 1.88–11.48 for 20 mg L^{-1} MO solution in the presence of 1.0 g L^{-1} adsorbent. The maximum decolorization percentage was found at pH 2.91. There was higher adsorption capacity of MO in acid solution because the swelling of composite films led to more available amino groups (–NH$_2$) and hydroxyl groups (–OH) in magnetic γ-Fe$_2$O$_3$/chitosan composite films. In addition, more protons were available to protonate amine groups in chitosan chains to form NH$_3$$^+$ at low pH (such as pH 2.91), increasing the number of binding sites for the adsorption of MO anions.[11] The adsorption capacity of MO on

Figure 5 Effect of solution pH on color removal of MO. $C_0 = 20$ mg/L, $m = 1$ g/L, agitation speed $= 100$ rpm, temperature $= 310$ K.
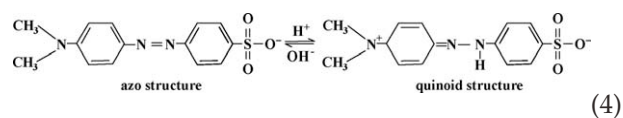

Figure 6 Effect of coexisting anions on color removal of MO. $C_0 = 20$ mg/L, $m = 1$ g/L, agitation speed $= 100$ rpm, temperature $= 310$ K, [coexisting anion] $= 0.01$ mol/L.

TABLE II
**Adsorption Kinetic Parameters for MO Adsorption on Magnetic γ-Fe$_2$O$_3$/Chitosan Composite Films
at Different Initial Dye Concentrations**

Initial Dye Concentration (mg/L)	$q_{e,exp}$ (mg g^{-1})	$q_{e1,cal}$ (mg g^{-1})	k_1 (min^{-1})	R^2	χ^2	$q_{e2,cal}$ (mg g^{-1})	k_2 (g mg^{-1} min^{-1})	R^2	χ^2
10	7.29	3.15	0.01368	0.949	21.980	7.61	0.007072	0.999	1.044
20	12.40	8.84	0.009857	0.989		13.32	0.00225	0.996	
30	18.85	13.27	0.008521	0.958		20.729	0.000935	1	
40	21.91	13.92	0.005711	0.980		24.15	0.000611	0.998	
50	25.06	18.30	0.006564	0.9985		28.22	0.00047	0.998	
60	28.54	18.35	0.005804	0.991		31.26	0.000486	0.995	

magnetic γ-Fe$_2$O$_3$/chitosan composite films was found to decrease from 20.02 to 11.37 mg g^{-1} with the increase in initial pH of MO solution from 2.91 to 9.38. This was due to the successive deprotonation of positive charged groups on the magnetic γ-Fe$_2$O$_3$/chitosan composite films and electrostatic repulsion between negatively charged sites on the composite films and MO molecules.[29] Furthermore, lower adsorption of the MO dye in alkaline medium was also due to the increased concentration of hydroxyl ions, which competed along with MO anions for binding sites on the surface of adsorbent. On the other hand, as expressed in equilibrium eq. (4), the quinoid structure of MO is more easily reduced than its azo structure.[30]

$$(4)$$

To our surprise, the removal percentage decreased to 50.23% when solution pH was further decreased to 1.88. One possible reason was due to the dissolution of uncrosslinked chitosan and γ-Fe$_2$O$_3$ at strong acidic environment. In fact, ∼ 4.6% weight of mag-

netic γ-Fe$_2$O$_3$/chitosan composite films was lost when the solution pH was 1.88 (Fig. 5).

Effect of coexisting anions

Various electrolytes are added to the dyeing bath in textile industries to improve color fastness,[31] which may affect the dye adsorption onto adsorbents. A total of 0.01 mol L^{-1} corresponding sodium salts was added into the prepared MO solutions of 20 mg L^{-1}. The effect of coexisting anions on MO adsorption is shown in Figure 6. As seen in Figure 6, the presence of inorganic salts has significantly retarded the adsorption rate of MO. In the presence of Cl$^-$, NO$_3^-$, CO$_3^{2-}$, and PO$_4^{3-}$, the removal percentage of MO solution were 42.83%, 33.11%, 9.45%, and 3.88% after 540 min, respectively, whereas 61.91% of dye removal was observed in the absence of anions. The inhibition effect may due to the competitive adsorption of inorganic anions with MO anions onto the surface of adsorbents. Of all the examined anions, the influence of phosphate ion was the strongest because the trivalent sodium phosphate (Na$_3$PO$_4$) had the most negative charges than the divalent electrolyte (Na$_2$CO$_3$) and the univalent electrolyte (NaCl and NaNO$_3$).[32]
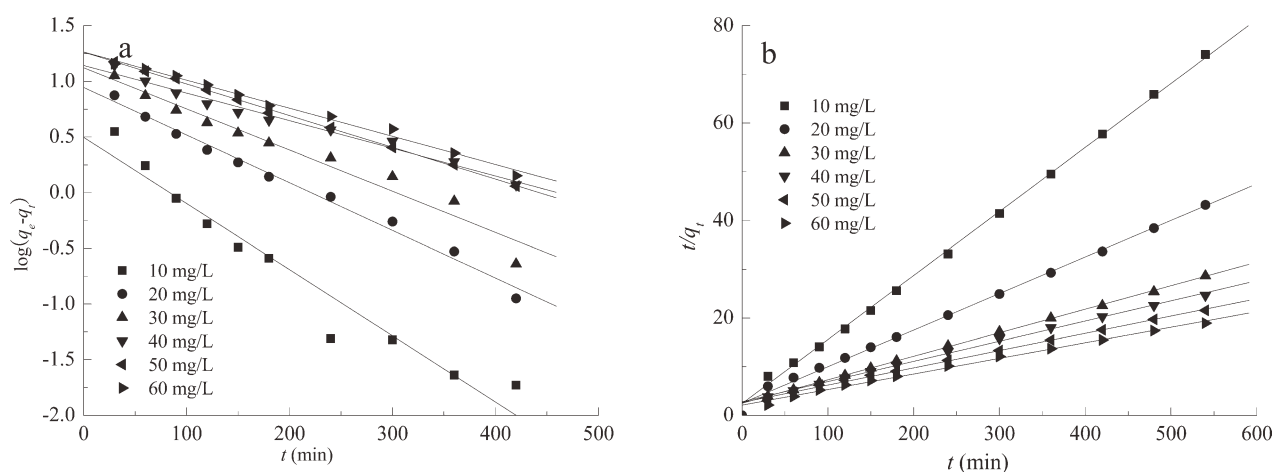

Figure 7 Plots of log(q_e-q_t) versus t (a) and t/q_t versus t (b) for MO adsorption at different initial dye concentrations.

Temperature (K)	Freundlich Isotherm				Langmuir Isotherm			
	K_F [mg/g (L/g)$^{1/n}$]	n	R^2	χ^2	q_m (mg/g)	K_L (L/mg)	R^2	χ^2
310	6.46	2.37	0.981	0.304	28.94	0.19	0.996	0.215
320	5.57	2.26	0.988	0.191	27.97	0.16	0.994	0.187
330	4.66	2.07	0.981	0.314	29.41	0.11	0.998	0.086

Adsorption kinetics

To investigate the controlling mechanism of the adsorption processes, pseudo-first-order and pseudo-second-order kinetic models were used to study the experimental data obtained.

The pseudo-first-order kinetic model is given as[33]

$$\log(q_e - q_t) = \log q_e - \frac{k_1}{2.303} t \tag{5}$$

where q_e and q_t are the amounts of MO adsorbed (mg g^{-1}) per unit of adsorbent at equilibrium and at time t, respectively. k_1 is the pseudo-first-order rate constant (min^{-1}). The rate constant (k_1) and correlation coefficients (R^2) are determined from the linear plots of $\log(q_e - q_t)$ versus t.

The pseudo-second-order kinetic model can be expressed as[34]

$$\frac{t}{q_t} = \frac{1}{k_2 q_e^2} + \frac{t}{q_e} \tag{6}$$

where k_2 is the pseudo-second-order rate constant of adsorption (g mg^{-1} min^{-1}). The linear plots of t/q_t versus t are used to determine the rate constant (k_2) and correlation coefficients (R^2).

The calculated kinetic parameters, their respective correlation coefficients and nonlinear χ^2 test are shown in Table II. Figure 7(a,b) shows the straight line plots of $\log(q_e - q_t)$ versus t and t/q_t versus t for different initial dye concentrations. As shown in Figure 7, the pseudo-first-order curves did not fit well with the experimental data, whereas the pseudo-second-order equation provided an excellent fit for the experimental data with a good linearization of all R^2 > 0.995. Moreover, the calculated $q_{e2,\text{cal}}$ values of pseudo-second-order equation were more close to those of experimentally obtained $q_{e,\text{exp}}$, confirming by a lower χ^2 value (Table II). Thus, it can be concluded that the adsorption of MO on magnetic γ-Fe$_2$O$_3$/chitosan composite films can be better explained by pseudo-second-order kinetic model and the process is chemical adsorption.

Adsorption isotherms

Equilibrium relationships between adsorbent and adsorbate are described by adsorption isotherms.

Two well-known adsorption isotherms were used in this study, namely the Freundlich and Langmuir isotherms. The Freundlich isotherm is used for a heterogeneous surface energy system. It is represented as[35,36]

$$q_e = K_F C_e^{1/n}. \tag{7}$$

Equation (7) can be linearized by taking logarithms:

$$\log q_e = \log K_F + \frac{1}{n} \log C_e \tag{8}$$

where C_e is the concentration of dye solution at adsorption equilibrium (mg L^{-1}), K_F [mg g^{-1} (L g^{-1})$^{-1/n}$] and n are the Freundlich constants related to the adsorption capacity and intensity, respectively.

The Langmuir isotherm equation is given as[22]

$$q_e = \frac{q_m K_L C_e}{1 + K_L C_e}. \tag{9}$$

Equation (9) can be linearized to the following equation:

$$\frac{1}{q_e} = \frac{1}{q_m} + \frac{1}{K_L q_m} \frac{1}{C_e} \tag{10}$$

where q_m is the maximum amount of adsorption which complete monolayer coverage on the adsorbent surface (mg g^{-1}), and K_L is the Langmuir binding constant, which is related to the energy of adsorption (L mg^{-1}).

The Freundlich and Langmuir isotherm constants, their respective correlation coefficients (R^2) and the χ^2 value were shown in Table III. As indicated by the correlation coefficients (R^2), both adsorption isotherm models fitted the experimental data. However, the results presented a better fit to the Langmuir equation with higher R^2 and smaller values of χ^2.

TABLE IV
R_L Values Based on the Langmuir Equation

C_0 (mg/L)	10	20	30	40	50	60
310 K	0.3438	0.2076	0.1487	0.1158	0.0949	0.0803
320 K	0.3877	0.2405	0.1743	0.1367	0.1124	0.0955
330 K	0.4710	0.3080	0.2288	0.1820	0.1511	0.1292

TABLE V
Thermodynamic Parameters for MO Adsorption on γ-Fe$_2$O$_3$/Chitosan Composite Films

Initial MO Concentrations (mg/L)	ΔS^o (J/mol K)	ΔH^o (kJ/mol)	ΔG^o (kJ/mol)		
			310 K	320 K	330 K
10	−53.74	−20.28	−3.62	−3.08	−2.54
20	−42.72	−15.72	−2.48	−2.05	−1.62
30	−33.95	−11.78	−1.26	−0.92	−0.58
40	−22.71	−7.59	−0.55	−0.32	−0.095

This indicated fully that the adsorption of MO onto the magnetic γ-Fe$_2$O$_3$/chitosan composite films was typical monomolecular layer adsorption and the nature of adsorption was chemisorption on a set of well-defined localized adsorption sites.

The Langmuir constant, K_L, can be used to determine a dimensionless separation factor,[37] R_L, to tell the favorability and the shape of the adsorption isotherms by applying the equation

$$R_L = \frac{1}{1 + K_L C_0} \qquad (11)$$

If the R_L values are equal to 0 or 1, the adsorption is either irreversible or linear, and if the values are between 0 and 1, adsorption is favorable to chemical adsorption.

As shown in Table IV, R_L approached 0 as C_0 increased. The values of R_L for three different temperatures were all less than 1 and greater than 0, indicating the favorable uptake of MO by the magnetic γ-Fe$_2$O$_3$/chitosan composite films. The lowest R_L of MO adsorption for whole ranges of dye concentration at 310 K indicated that MO adsorption on the magnetic γ-Fe$_2$O$_3$/chitosan composite films was more favorable at lower temperature. This was in agreement with the experiment results of effect of temperature.

Thermodynamic parameters

The Gibb's free energy (ΔG^o), entropy (ΔS^o) and enthalpy (ΔH^o) changes for the adsorption were determined by[22]

$$\Delta G^o = \Delta H^o - T\Delta S^o, \qquad (12)$$

$$\log K_c = \frac{\Delta S^o}{2.303R} - \left(\frac{\Delta H^o}{2.303R}\right)\frac{1}{T} \qquad (13)$$

where K_c, the thermodynamic equilibrium constant, is the ratio of the amount adsorbed per unit mass (q_e) to the solute concentration in solution (C_e) at equilibrium. R is the ideal gas constant, and T is the adsorption temperature in Kelvin.

The ΔS^o and ΔH^o values were obtained from the slope and intercept of the straight line of plots of $\log(q_e/C_e)$ versus $1/T$, respectively. The plots of

$\log(q_e/C_e)$ versus $1/T$ have shown good linearity with very good coefficients ($R^2 > 0.99$). The thermodynamic parameters computed for the present case in the studied solute concentrations are given in Table V.

The negative values of ΔH^o further confirmed the exothermic nature of the process, whereas the negative values of ΔS^o suggested a decrease in randomness at the solid/solution interface during the adsorption. The values of ΔG^o were negative, confirming the feasibility of the process and the spontaneous nature of the adsorption process. It had been found that with increase in temperature, adsorption capacity decreased. The observed shifts in magnitude of ΔG^o to higher negative values at lower temperature were indicative of a rapid and more spontaneous adsorption with decreasing temperature,[20] which may also be reflected in the value of K_L. The values of K_L increased as the temperature decreased, indicating higher affinity of the magnetic γ-Fe$_2$O$_3$/chitosan composite films towards MO at lower temperature.

Magnetic recovery

It is very important for the industrial application to be recovered easily from the treated wastewater. As

Figure 8 Paragraphs of magnetic γ-Fe$_2$O$_3$/chitosan composite films dispersed in dye solution (left) and the response to a magnetic field (right). [Color figure can be viewed in the online issue, which is available at wileyonlinelibrary.com].

TABLE VI
Comparison of the Adsorption Capacity of γ-Fe$_2$O$_3$/Chitosan Composite Films with Other Adsorbents

Adsorbents	q_{max} (mg g^{-1})	Reference
Alginate/polyaspartate hydrogels	0.22–0.28	38
Alginate	0.08–0.28	38
Bottom ash	3.618	39
De-oiled soya	16.664	39
Orange peel	20.0	40
Banana peel	21.0	40
γ-Fe$_2$O$_3$/chitosan composite films	29.41	This study
γ-Fe$_2$O$_3$/MWCNTs/chitosan	60.5–66.1	22
Hypercrosslinked polymeric adsorbent(HJ-1)	70.9–76.9	41

shown in Figure 8 (left), the prepared magnetic γ-Fe$_2$O$_3$/chitosan composite films could be readily dispersed in water under stirring. What is more, the nanocomposite films have sensitive magnetic response to an adscititious magnetic field. As shown in Figure 8 (right), the nanocomposite films were easily separated from treated aqueous solution within 10 s by placing a permanent magnet near the sidewall of the glass. The excellent magnetic responsivity was necessary for magnetic separation to recovery of nanocomposite adsorbent from treated effluents in practical application.

Comparison with other adsorbents

A comparison of the maximum adsorption capacity (q_{max} value) for MO on γ-Fe$_2$O$_3$/chitosan composite films with those of other adsorbents reported by other researchers is shown in Table VI. The adsorption capacity of γ-Fe$_2$O$_3$/chitosan composite films was higher than those of alginate,[38] polyaspartate hydrogels,[38] bottom ash,[39] de-oiled soya,[39] banana peel,[40] and orange peel,[40] while was lower than those of γ-Fe$_2$O$_3$/MWCNTs/chitosan[22] and hypercrosslinked polymeric adsorbent (HJ-1).[41] Generally, the γ-Fe$_2$O$_3$/chitosan composite films was suitable and promising for the removal of MO from aqueous solutions because it has a relatively higher adsorption capacity than many low-cost adsorbents.

CONCLUSIONS

In this study, magnetic γ-Fe$_2$O$_3$/chitosan composite films were prepared by solution casting method based on the highly viscous nature and excellent film forming property of chitosan. FTIR, TG-DSC, and XRD analysis were performed to confirm the observed results. Batch adsorption experiments were carried out utilizing the composite films to adsorb MO from aqueous solutions. The effects of adsorbent dosage, solution pH, coexisting anions, and temperature were studied. Adsorption kinetic was verified by pseudo-first-order and pseudo-second-order models. Results indicated that the rate of dye adsorption followed pseudo-second-order kinetic model for the initial dye concentration range studied in the present case. MO adsorption onto magnetic γ-Fe$_2$O$_3$/chitosan composite films was better described by the Langmuir isotherm. The separation factor in the study was $0 < R_L < 1$, indicating the favorable uptake of MO onto the magnetic γ-Fe$_2$O$_3$/chitosan composite films. Thermodynamic studies showed the MO adsorption process was exothermic and spontaneous in nature.

NOMENCLATURE

a	Initial adsorption rate constant, mg g^{-1} min^{-1}
C	Liquid-phase concentration at any time, mg L^{-1}
C_0	Initial liquid-phase concentration, mg L^{-1}
C_e	Equilibrium liquid-phase concentration, mg L^{-1}
k_1	Rate constant of pseudo-first-order adsorption, min^{-1}
k_2	Rate constant of pseudo-second-order adsorption, g mg^{-1} min^{-1}
k_L	Langmuir binding constant, L mg^{-1}
m	Mass of adsorbent, g
q_t	Solid-phase concentration at any time, mg g^{-1}
q_e	Equilibrium solid-phase concentration, mg g^{-1}
$q_{e,cal}$	Calculated equilibrium capacity from the isotherm model, mg g^{-1}
$q_{e,exp}$	Equilibrium adsorption capacity from the experiment, mg g^{-1}
R^2	Coefficient of correlation
Q_0	Langmuir equilibrium constant, mg g^{-1}
t	Time, min
T	Temperature, °C (K)
V	Volume of solution, L

Greek symbols

λ	Wavelength, nm
η	Decolorization rate, %

References

1. Chiou, M. S.; Ho, P. Y.; Li, H. Y. Dyes Pigments 2004, 60, 69.
2. Razo-Flores, E.; Luijten, M.; Donlon, B.; Lettinga, G.; Field, J. Water Sci Technol 1997, 36, 65.
3. Kim, T. H.; Park, C. W.; Kim, S. Y. J Cleaner Prod 2005, 13, 779.
4. Zeng, Y.; Yang, C.; Zhang, J.; Pu, W. J Hazard Mater 2007, 147, 991.
5. Nataraj, S. K.; Hosamani, K. M.; Aminabhavi, T. M. Desalination 2009, 249, 12.
6. Lachheb, H.; Puzenat, E.; Houas, A.; Ksibi, M.; Elaloui, E.; Guillard, C.; Herrmann, J. M. Appl Catal B: Environ 2002, 39, 75.
7. Annadurai, G.; Ling, L. Y.; Lee, J. F. J Hazard Mater 2008, 152, 337.

8. Kyzas, G. Z.; Lazaridis, N. K. J Colloid Interface Sci 2009, 331, 32.

9. Zhou, L. M.; Wang, Y. P.; Liu, Z. R.; Huang, Q. W. J Hazard Mater 2009, 161, 995.

10. Chen, C. L.; Hu, J.; Shao, D. D.; Li, J. X.; Wang, X. K. J Hazard Mater 2009, 164, 923.

11. Li, G. Y.; Jiang, Y. R.; Huang, K. L.; Ding, P.; Yao, L. L. Colloids Surf A 2008, 20, 11.

12. Qu, S.; Huang, F.; Yu, S. N.; Chen, G.; Kong, J. J. J Hazard. Mater 2008, 160, 643.

13. Zhao, S.; Asuha, S. Powder Technol 2010, 197, 295.

14. Pan, J.; Yao, H.; Li, X.; Wang, B.; Huo, P.; Xu, W.; Ou, H.; Yan, Y. J Hazard Mater 2011, 190, 276.

15. Zhu, H. Y.; Jiang, R.; Xiao, L. Appl Clay Sci 2010, 48, 522.

16. Nakamae, K.; Yamaguchi, K.; Sumiya, K.; Kitagawa, S. J Adhes 1994, 45, 259.

17. El-Shobaky, G. A.; Fagal, G. A.; El-Shobaky, H. G.; El-Khouly, S. M. Colloids Surf A 1999, 152, 275.

18. Zhu, H. Y.; Jiang, R.; Xiao, L.; Li, W. J Hazard Mater 2010, 179, 251.

19. Ho, Y. S. Carbon 2004, 42, 2115.

20. Vimonses, V.; Lei, S. M.; Jin, B.; Chow, C. W. K.; Saint, C. Appl Clay Sci 2009, 43, 465.

21. Chatterjee, S.; Lee, D. S.; Lee, M. W.; Woo, S. H. Bioresour Technol 2009, 100, 2803.

22. Zhu, H. Y.; Jiang, R.; Xiao, L.; Zeng, G. M. Bioresour Technol 2010, 101, 5063.

23. Douglas, B.; Paulo, C. F. S. Thermochim Acta 2007, 465, 73.

24. Ma, G. P.; Yang, D. Z.; Kennedy, J. F.; Nie, J. Carbohydr Polym 2009, 75, 390.

25. Zhang, T. S.; Luo, H. M.; Zeng, H. X.; Zhang, R. F.; Shen, Y. S. Sens Actuators B 1996, 32, 181.

26. Cao, S. W.; Zhu, Y. J.; Zeng, Y. P. J Magn Magn Mater 2009, 321, 3057.

27. Fan, X.; Tan, F.; Zhang, G.; Zhang, F. Mater Sci Eng A 2007, 454–455, 37.

28. Ngah, W. S. W.; Fatinathan, S. Chem Eng J 2008, 143, 62.

29. Senthil Kumar, P.; Ramalingam, S.; Senthamarai, C.; Niranjanaa, M.; Vijayalakshmi, P.; Sivanesan, S. Desalination 2010, 261, 52.

30. Chemie, V. F. PhD thesis, Duisburg University, Germany, 2005.

31. Riga, A.; Soutsas, K.; Ntampegliotis, K.; Karayannis, V.; Papapolymerou, G. Desalination 2007, 211, 72.

32. Maurya, N. S.; Mittal, A. K.; Cornel, P.; Rother, E. Bioresour Technol 2006, 97, 512.

33. Lagergren, S. Kungliga Svenska Vetenskapsakademiens Handlingar 1898, 24, 1.

34. Ho, Y. S.; McKay, G. Process Biochem 1999, 34, 451.

35. Yasemin, B.; Numan, G.; Haluk, A. J Hazard Mater 2007, 144, 300.

36. Sun, Q.; Yang, L. Water Res 2003, 37, 1535.

37. Hall, K. R.; Eagleton, L. C.; Acrivos, A.; Vermeulen, T. Ind Eng Chem Fundam 1966, 5, 212.

38. Jeon, Y. S.; Lei, J.; Kim, J. H. J Ind Eng Chem 2008, 14, 726.

39. Mittal, A.; Malviya, A.; Kaur, D.; Mittal, J.; Kurup, L. J Hazard Mater 2007, 148, 229.

40. Annadurai, G.; Juang, R. S.; Lee, D.-J. J Hazard Mater 2002, 92, 263.

41. Huang, J. H.; Huang, K. L.; Liu, S. Q.; Wang, A. T.; Yan, C. Colloids Surf A 2008, 330, 55.